Tidal control of jet eruptions on Enceladus as observed by Cassini ISS between 2005 and 2007

T.A. Hurford [a,*], P. Helfenstein [b], J.N. Spitale [c]

[a] Planetary Systems Laboratory, NASA Goddard Spaceflight Center, Greenbelt, MD 20771, USA
[b] CRSR, Cornell University, Ithaca, NY 14853, USA
[c] Planetary Science Institute, 1700 E. Ft. Lowell, Suite 106, Tucson, AZ 85719, USA

ARTICLE INFO

ABSTRACT

Observations of Enceladus have revealed active jets of material erupting from cracks on its south polar surface. It has previously been proposed that diurnal tidal stress, driven by Enceladus' orbital eccentricity, may actively produce surface movement along these cracks daily and thus may regulate when eruptions occur. Our analysis of the stress on jet source regions identified in Cassini ISS images reveals tidal stress as a plausible controlling mechanism of jet activity. However, the evidence available in the published and preliminary observations of jet activity between 2005 and 2007 may not be able to solidify the link between tidal stress and eruptions from fissures. Ongoing, far more comprehensive analyses based on recent, much higher resolution jetting observations have the potential to prove otherwise.

Published by Elsevier Inc.

1. Introduction

Observations by Cassini's Imaging Science Subsystem (ISS) of Enceladus' south polar region at high phase angles have revealed jets of material venting into space (Porco et al., 2006). Observations by Cassini's Composite Infrared Spectrometer (CIRS) have also shown that the south polar region is anomalously warm in hotspots associated with geological features called the Tiger Stripes (Spencer et al., 2006; Porco et al., 2006). The Tiger Stripes are large rifts near the south pole of Enceladus, which are typically about 130 km in length, 2 km wide, including a central trough 500 m deep flanked on each side by 100 m tall ridges (Porco et al., 2006). Preliminary triangulation of jets as viewed at different times between 2005 and 2007 and with different viewing geometries in Cassini ISS images have pinpointed the locations of eight major eruptions of material and found all of them on the south polar Tiger Stripes fractures. Four of them are coincident with the hotspots reported in 2006 by CIRS (Spitale and Porco, 2007).

While published ISS observations of jets suggest that individual eruption sites stay active on the timescale of years, any shorter temporal variability (on timescales of an orbital period, or 1.3 Earth days, for example) is more difficult to establish because of the spotty temporal coverage and the difficulty of visually isolating one jet from the forest of many seen in a typical image. Consequently, it is not known whether any individual jet is continuously active, randomly active, or whether they erupt on a predictable, periodic schedule.

One mechanism that may control the timing of eruptions is diurnal tidal stress, which oscillates between compression and tension at any given location throughout Enceladus' orbit and may allow the cracks to open and close periodically (Hurford et al., 2007a). The main source of diurnal stress arises from the moon's orbital eccentricity. Thus, examination of the diurnal time variability in the magnitude of jet eruptions across the south polar terrain has the potential to offer insights into the rotation state of the moon.

In this paper, we first summarize the early observations of jet activity as presented by Spitale and Porco (2007) and place those observations into Encealdus' orbital context. Then using the techniques outlined by Hurford et al. (2007a, 2009a), we examine the stresses on the Tiger Stripe regions to see how well diurnal tidal stress caused by Enceladus' orbital eccentricity correlates with the observed eruptions. We then identify possible mechanisms by which tidal stress can control access to the surface for volatile material and implications for observed jet activity.

2. Observations of jets from Enceladus

The location of jets originating from the south polar region of Enceladus were determined by Spitale and Porco (2007) via triangulation using multiple observations by ISS from February 2005 to April 2007. Table 1 summarizes these observations and the results of Spitale and Porco (2007), showing the sources identified with each observation.

---

* Corresponding author.
E-mail address: terry.a.hurford@nasa.gov (T.A. Hurford).

Table 1
Observations of jet activity on Enceladus.

Observation name (Cassini designation)	Time span of observation	Observation designation[a]	Active sources[a] identified	Enceladus' mean anomaly (°)
ISS_003EN_PLUME001_PRIME	2005-048T11:49:48 2005-048T12:15:02	C	SI, SIV, SVI	342.1–345.6
ISS_018EN_HIPHAS001_PRIME	2005-331T17:03:10 2005-331T17:34:31	A	SI, SII, SIII, SV, SVI, SVII, SVIII	113.3–122.2
ISS_018EN_PLUMES001_PRIME	2005-331T19:03:10 2005-331T19:34:04	B	SII, SIII, SIV	140.8–148.6
ISS_020EN_094W151PH001_PRIME	2006-018T17:25:17 2006-018T17:43:12	D	SII	80.3–83.4
ISS_020EN_166W154PH001_PRIME	2006-018T23:30:58 2006-018T23:47:14	E	SII, SIV	159.4–163.7
ISS_022EN_022W159PH001_PRIME	2006-081T09:55:09 2006-081T10:11:51	G	SI, SII, SIII, SIV, SV, SVI, SVII, SVIII	351.2–353.6
ISS_022EN_022W162PH001_PRIME	2006-082T20:14:19 2006-082T20:31:28	H	SII, SIII, SVI, SVII	2.6–5.0
ISS_022EN_238W162PH001_PRIME	2006-083T14:35:59 2006-083T14:53:07	I	SI	214.5–218.7
ISS_023EN_238W163PH001_PRIME	2006-123T08:25:39 2006-123T08:38:16	J	SI, SVII	198.3–201.7
ISS_023EN_310W163PH001_PRIME	2006-123T14:48:38 2006-123T15:02:16	K	SIV, SVIII	281.0–283.2
ISS_023EN_094W157PH001_PRIME	2006-124T05:21:39 2006-124T05:34:38	L	SIII, SV	46.8–48.7
ISS_023EN_166W159PH001_PRIME	2006-124T11:32:39 2006-124T11:45:39	M	SIII	110.5–113.3
ISS_027EN_166W164PH001_PRIME	2006-223T03:34:46 2006-223T03:49:15	N	SI, SII	79.6–82.0
ISS_028RI_HIPHWAC001_PRIME	2006-258T17:11:38 2006-258T17:13:13	O	SI, SIII	55.3–55.4
ISS_043EN_PLUMES001_PRIME	2007-114T14:40:29 2007-114T15:21:29	T	SIII, SV, SVII	56.0–62.4

[a] Spitale and Porco (2007).

Every time ISS has observed the south pole at high phase angles, it has witnessed plumes. When the resolution is adequate, individual jets can be distinguished. These observations imply continual activity, but not necessarily that any individual jet remains constantly active. In fact, Spitale and Porco (2007) note that Source I is not visible in observation K even though the viewing geometry should be favorable for its detection. Even though image resolution for observation K may limit the ability to detect activity from Source I, in general, the activity of an individual jet source may be variable. Here we consider whether periodic variation of tidal stress might influence the timing of jet activity.

In order to address this question, the observations must be placed into the context of Enceladus' orbit. Based on the time of each observation, the orbital location of Enceladus within its orbit with reference to pericenter (the"mean anomaly") is also shown in Table 1. Based on those data, Fig. 1 summarizes the relationship between the mean anomaly and plume activity. In this figure, the acquisition times of the 15 imaging sets (A–T, as identified along the top of the figure) are shown as shaded regions with respect to Enceladus' mean anomaly on the horizontal axis. The figure is divided vertically into 8 portions, corresponding to the eight sources (SI–SVIII) identified by Spitale and Porco (2007), ordered based on the Tiger Stripe with which the source is associated. If a source was active in a particular image set, the shaded region is green. It is important to note the following points about the data set:

First, the 15 observations do not provide uniform coverage of jet activity throughout Enceladus' orbit. Of the 15 observations two-thirds (10) of them fell within the first half of Enceladus' orbit, while one-third (5) sampled the second half of the orbit. At none of these times did jet activity cease altogether.

Second, one pair of observations (N&D) overlap in time relative to Enceladus' orbit, although they were taken seven months apart. Source II was observed to be active at both times, but Source I was only active during one of these two observations (N, but not D).

Since tidal stress would be the same during both orbits, this would seem to contradict the tidal hypothesis. However, the null result during D may not be reliable. As shown by Spitale and Porco (2007 supplementary information) the geometry of observation D could have hidden activity at Source II due to an alignment with Source I.

Third, the pair of observations M&A are contiguous in mean anomaly, providing a continuous coverage over the combined time span, beginning about one third of an orbit past pericenter. While most sources were active during observation A, only Source III is observed to be active during M. This is likely an observational effect, because observation M is not of equal quality to A: some jets could have been missed by observation M.

Fourth, the pair of observations O&T, which were taken eight months apart, nearly span a contiguous range of mean anomaly at about a sixth of Enceladus' orbit. Only Source III was observed to be active during both observation periods. Source I was active during O but not T, while Sources V and VII are active in T but not O. Again, the supplementary information of Spitale and Porco (2007) suggests that observation O may be limited in its ability to identify plumes because of the observation geometry and range.

Therefore, we assume for purposes of our study that the null results for Sources V and VII during observation O, for all sources during M, and for Source I during observation D should be ignored.

In Fig. 2, the regions consistent with the locations of the eight sources identified by Spitale and Porco (2007) are shown with respect to the Tiger Stripes. Sources I, II, III and VI correspond to locations along Damascus Sulcus and Baghdad Sulcus where Cassini CIRS has observed the hottest temperatures and thus the greatest power emitted from the surface (Howett et al., 2011). Sources IV, VII and VIII are associated with warmer regions along their Tiger Stripes, but since the eight sources identified by Spitale and Porco (2007) are likely to be the combined output from numerous smaller sources at higher resolution (Porco et al., 2011), the location of activity consistent with Sources IV, VII and VIII is not well
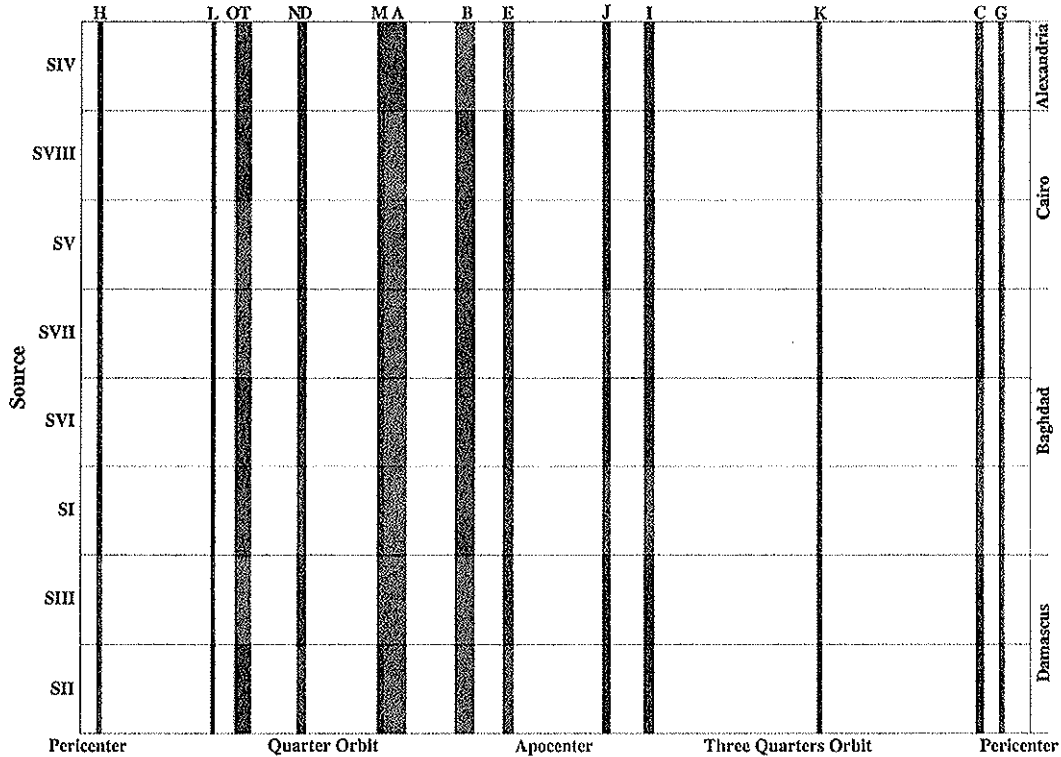
Fig. 1. Orbital context for jet observations. From Table 1 each Cassini ISS observation of active jets on Enceladus are placed into an orbital context based on the time of the observations and the location of Enceladus in its orbit. The observations are shown as shaded bars where they occur in the orbit and are label by a letter designation as shown on the top of the plot (Spitale and Porco, 2007). Furthermore, each shaded bar is broken into eight regions for each source identified by Spitale and Porco (2007). If Spitale and Porco (2007) deemed the source to be producing an active jet, the bar is shaded green.

constrained. Moreover, Source V is offset from the warmest region detected by CIRS suggesting its triangulated location may not be as reliable. Therefore, here we assume that positive detections of plumes for Sources I, II, III and VI are reliable and are very confident about our identification of the portion of the Tiger Stripe from which these sources radiate. Moreover, Sources I, II and III showed the greatest activity in Spitale and Porco (2007). Thus, we focus on the stress along the Tiger Stripes in the regions consistent with these four Sources (I, II, III and VI) and on this basis we compare various models for tidal variation with the observational record. In Fig. 2 for Sources I, II, III and VI we show these regions in dark gray, and we highlight (in light gray) the portions of the Tiger Stripes consistent with observed source locations for I, II, III and VI. We assume that observed jets originate from the Tiger Stripes within these highlighted segments.

3. Modeling of tidal stress at source locations

Enceladus' finite orbital eccentricity causes small daily changes in the distance between Enceladus and Saturn, affecting the height of the tide raised on the satellite by the planet. During an orbit, the height of the main tide oscillates with an amplitude $(9eh_2MR)/(4\pi\rho_{av}a^3)$ where e is the orbital eccentricity h_2 is the Love number describing the radial response of the body to the tide raising potential, M is the mass of the tide-raiser (in this case Saturn), R is Enceladus' radius, ρ_{av} is the average density of Enceladus and a is the semi-major axis of its orbit, which describes the average distance to Saturn. In addition to affecting the height of the tide on Enceladus, the orbital eccentricity also causes the longitude of the tidal bulge to oscillate as it tracks the position of Saturn throughout an orbit. This constant reshaping of Enceladus as it orbits Saturn stresses its surface.

To approximate the surface stresses from the tidal deformation of an elastic outer layer, we assume that the icy shell is thin and that it is effectively decoupled from the deeper interior of Enceladus. In other words, there is negligible shear between the thin elastic shell and the interior, as for example in the presence of a global subsurface ocean (Sohl et al., 2006; Zhang and Nimmo, 2009; Patthoff and Kattenhorn, 2011). A thin elastic outer layer cannot significantly affect the tidal distortion of Enceladus and thus it deforms to fit the tidal figure taken by the interior, stretching and producing stress on its surface. These stresses are given by the Vening–Meinesz equations:

$$\sigma_{\theta\theta} = \frac{3Mh_2\mu}{8\pi\rho_{av}a^3}\left(\frac{1+\nu}{5+\nu}\right)(5+3\cos 2\theta) \tag{1}$$

and

$$\sigma_{\phi\phi} = -\frac{3Mh_2\mu}{8\pi\rho_{av}a^3}\left(\frac{1+\nu}{5+\nu}\right)(1-9\cos 2\theta) \tag{2}$$

where θ is a surface point's angular distance from the axis of symmetry with respect to the tidal deformation (Melosh, 1977; Leith and McKinnon, 1996; Greenberg et al., 1998). The tidal axis of symmetry is along a line connecting the center of Enceladus and the center of Saturn. In these expressions μ is the rigidity of the thin elastic shell while ν is its Poisson ratio. The stress along the surface in a direction along the great circle connecting that point to the axis of symmetry is given by $\sigma_{\theta\theta}$, while $\sigma_{\phi\phi}$ is the stress along the surface in a direction orthogonal to $\sigma_{\theta\theta}$. In the convention used here positive stresses are tensile and negative stresses compressional.

For a water–ice crust, we adopt plausible values for the elastic parameters of $\mu = 3.52 \times 10^9$ Pa and $\nu = 0.33$. We assume a conservative value for the tidal response given by $h_2 = 0.32$, which corresponds to a diurnal tidal amplitude (daily change in radius) of
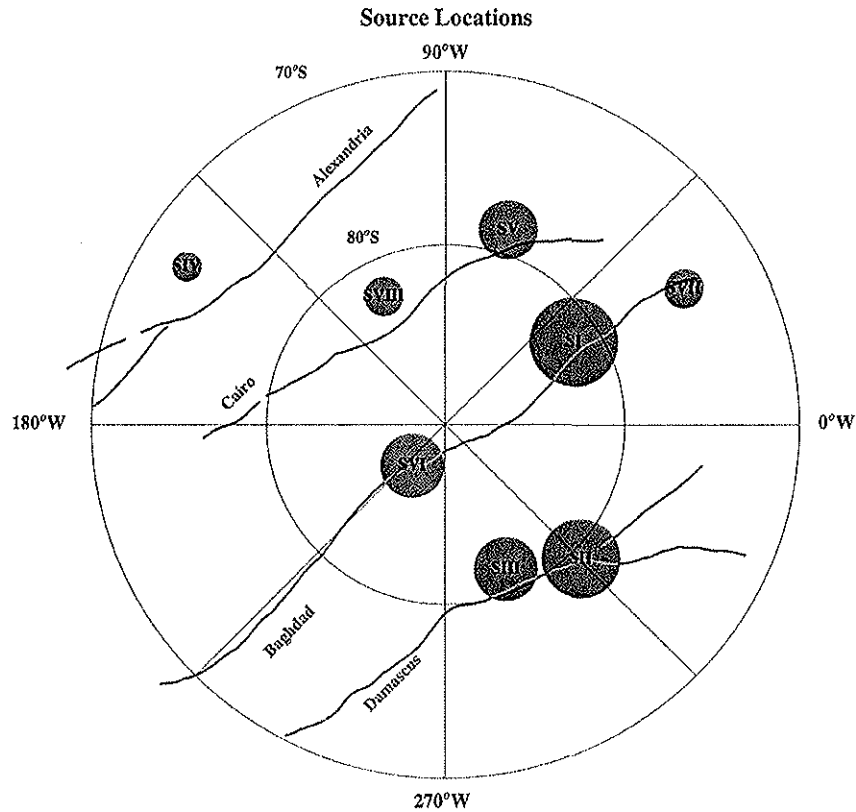
Source Locations

Fig. 2. Source locations with respect to Tiger Stripe cracks. The four major Tiger Stripe features are shown in the south polar region of Enceladus. The circles indicate possible source regions for active jets as identified by Spitale and Porco (2007) and are labeled with a source number designation. The size of these circles is associated with the uncertainty in the triangulation methods employed by Spitale and Porco (2007). When exploring the role of tidal stress on the Tiger Stripes associated with each source region, we focus on the portions of Tiger Stripes (shown in light gray) that lie within the possible source regions of Sources I, II, III, and VI.

~5 m when $e = 0.0047$ and $\rho_{av} = 1608$ kg/m^3. This value of h_2 yields maximum stresses on the order of 1 bar or 10^5 Pa, comparable to the tensile strength of ice. On Europa, stresses of this order are thought to control tensile failures in its icy crust (Hoppa et al., 2001, 2007b). We assume that stresses of this magnitude would also allow for tensile failure on Enceladus.

Following the methods of Hurford et al. (2009a), Eqs. (1) and (2) can be used to find stress at any latitude and longitude on Enceladus' surface throughout its orbit. For any crack with a known position and orientation, the tidal stresses can be decomposed into three components: one perpendicular to the crack, one parallel to the crack and a third that shears the two sides of the crack. In this paper, we focus on the stresses perpendicular to the crack, which may serve to pull the crack open in tension and push it closed in compression (Hurford et al., 2007a). Then we compare observations of active jets with the times that those tiger-stripe cracks at the source locations are under tension according to the tidal model.

4. Tidal control of jet eruptions by eccentricity-driven diurnal tides

We first characterize the tidal stress on the Tiger Stripes segments contained within source regions I, II, III and VI, over the course of Enceladus' orbit, assuming orbital eccentricity is the only source for the stress. Fig. 3 summarizes the results for each of the four source regions, superimposed on the observational results from Fig. 1. Here the maximum tensile stress and the maximum absolute shear stress experienced in the Tiger Stripe source regions are shown along with the theoretical percent of the region in tension, as a function of orbital position. For each source region, the Tiger Stripe first experiences tension shortly after pericenter, and

in most cases the transition from compression to tension is rapid. By the time Enceladus reaches apocenter, each source region is completely in tension. After apocenter passage the stresses become more compressional, until pericenter passage, when the cycle repeats.

The majority of the observations of jet activity occur when each source region is in tension. Of the 26 detections of activity among the four source regions (I, II, III, and VI), 17 detections or 65% occur at times when the source region is in tension (Fig. 3). This may be a result of the fact that jet observations are more likely to fall in the first half of the orbit when cracks are predicted to experience tension. However, observation G consistently shows activity for each source region at a time when each region is predicted to experience compression. Moreover, observations H&C show a similar result, although these observations may not be as reliable (Spitale and Porco, 2007). In all, 9 or 35% observations occur when compression is predicted in their source regions. Of these 9, 7 occur while the maximum tension predicted is increasing in their source regions.

Throughout the orbit at all source regions, the maximum absolute shear stress experienced remains fairly steady at about half a bar (Fig. 3). During the orbit the shear stress oscillates between right and left lateral senses of shear and the magnitude of shear changes at any given location, but the maximum absolute shear remains somewhat steady over the source region. The average value of the absolute shear throughout the orbit is consistent with previous studies (Hurford et al., 2009a), which confirmed that source regions are places along the Tiger Stripes that experience greater than average absolute shear (Nimmo et al., 2007).

With the characterization of the tidal stress throughout the orbit and the observations of jet activity, we can investigate whether

(a)

Source II
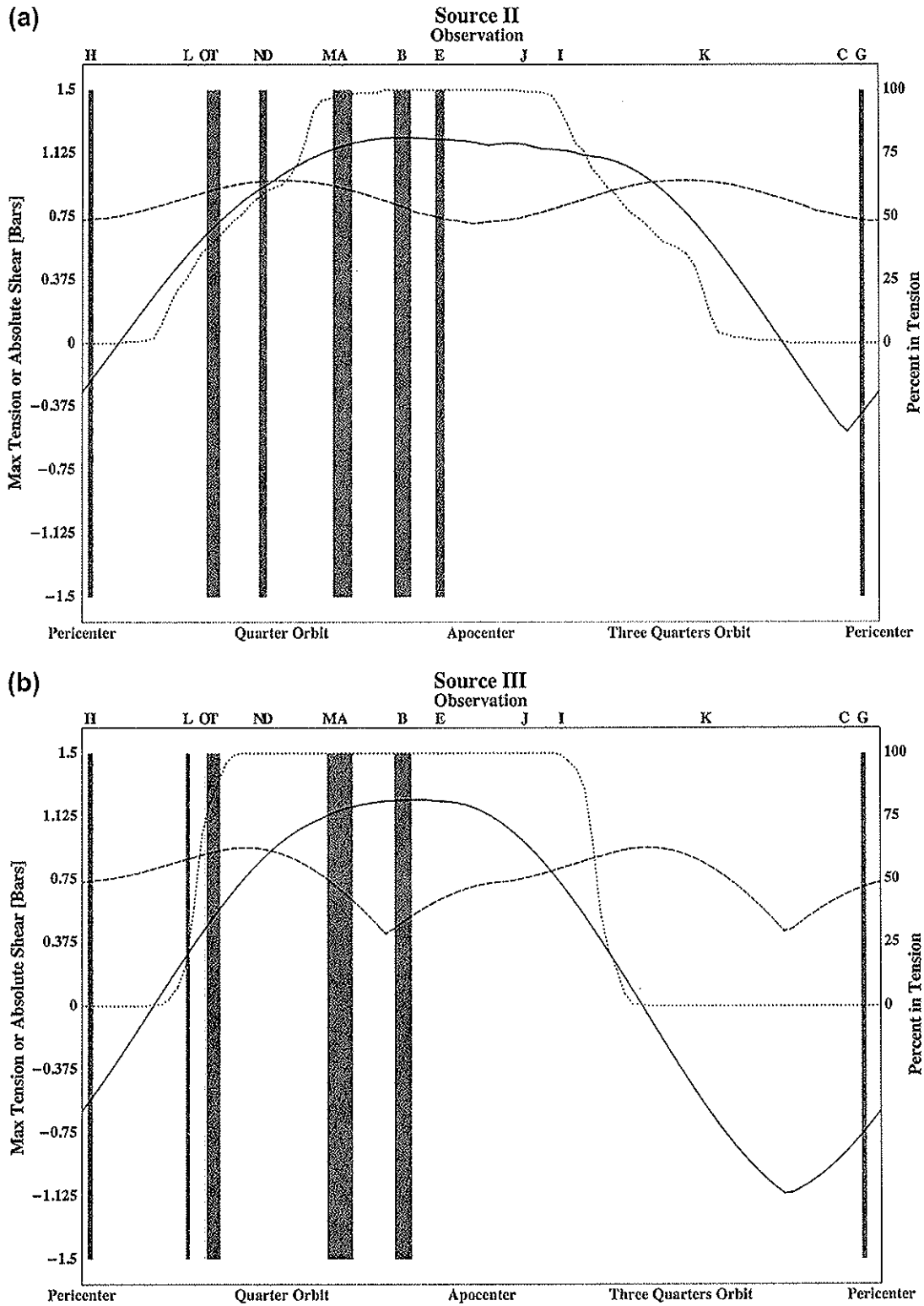Observation

(b)

Source III
Observation

Fig. 3. Activity at each source region with eccentricity driven tidal stress only. For the four source regions along Baghdad and Damascus Sulcus that are the focus of this paper, the maximum tensile stress (solid line) and the absolute shear stress (dashed line) experienced by any part of each source region are shown throughout the orbit along with the fraction of the region experiencing tensile stresses across the fracture (dotted line). For comparison to the observations of jet activity, green shaded bars are shown where activity was detected by Spitale and Porco (2007) (as in Fig. 1).

tidal stress can influence geological activity and control the eruptions of observed jets. In order for jet activity to occur, a conduit must be established from the surface to a subsurface reservoir of volatile material. This can be done by (1) tensile stresses directly opening a conduit or by (2) shear failure displacement opening conduits.
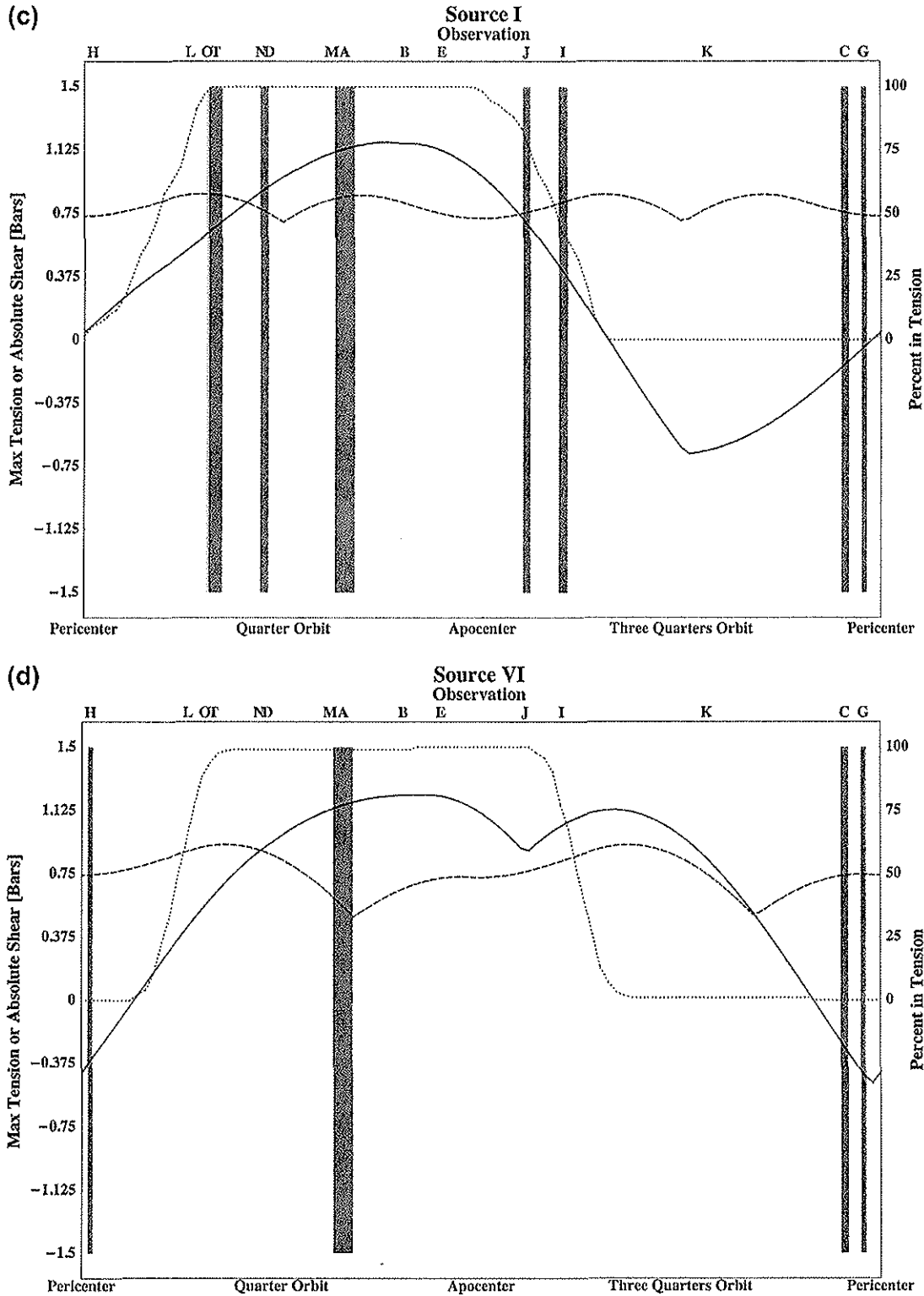
(c)

(d)

Fig. 3 (continued)

Under the assumption that fissures can actively erupt material only while in tension and can remain active as long as the conduit remains open, the majority of the observations of jet activity do occur when each source region is in tension. However, some observations show activity for source regions at times when those regions are predicted to experience compression. It may be that the assumption of eruptions coinciding with just conditions of tidal tensile stress may be too simplistic. For example, if a subsurface head of volatile material were to build up while a fracture is in compression, significant activity may be possible as soon as a crack

begins to experience tension as long as the built up pressure can overcome compressive forces. Indeed, we see that even while in compression, source regions experience minimal compression compared to the levels of tension they experience. Thus, in some regions tidal compression may not be enough to prohibit jet activity altogether. In fact, under the assumption that tidal activity is possible as long as a fracture is transitioning to greater tensile stress or experiencing tensile stress, 92% of the observations would be explained.

Thus far, we have focused on the link between tension and jet activity, however tidal shear stress may also play a role in eruption activity. Even when a fracture is experiencing compression, shear stress, if large enough, can produce slip along the fault (Smith-Konter and Pappalardo, 2008). If the fault walls were completely smooth and of constant orientation then slip would not produce conduits for volatile escape. However, real fault walls are not smooth and do vary in orientation. Thus, during slip failures openings may form, allowing trapped volatiles to escape and produce jets above the surface. This provides another mechanism to allow observed jet activity to occur even under periods of compression. This mechanism may be best to explain observed activity at Source VI during observations C&G. At these times, jet activity is observed while the fracture is experiencing compression, but the magnitude of the shear stress is greater than the compressive stress by over a factor of 2, making near surface slip possible even if friction along the fault is high.

Tidal stress conditions exist along the Tiger Stripes that would enable jet activity to occur at the times Cassini ISS observed activity in the 2005–2007 time frame, and the idea that tidal stress can control jet activity is plausible. However, the preliminary observations thus far may not be able to adequately prove the link between the two.

5. Discussion and conclusions

We have focused on the published observations of jet activity from 2005 to 2007, which were used by Spitale and Porco (2007) to triangulate jet source locations. However, the preliminary low-resolution observations published thus far are inadequate to prove definitively the link between the two. Since 2007, there have been many more observations of jet activity with higher-resolutions and further links between tidal stress and jet activity might be possible.

In order to solidly establish the link, analysis of jet observations should focus on the following. First, if possible, observations should focus on times in Enceladus' orbit between apocenter and pericenter passage. This portion of the orbit has not been well characterized by past observations and must be filled in to ensure that any link is not biased by an observational selection effect. Also, times in Enceladus' orbit when jet activity has already been observed should be retargeted to confirm that this activity is consistent at those points in the orbit.

Second, observations of inactivity at a source region are just as important as positive detections of activity. Future observations should attempt to determine whether individual source regions are inactive and whether this inactivity repeats in a predictable cycle. A good characterization of both activity and non-activity throughout the orbit will definitely limit the possible processes of tidal control of eruptions and solidify the link between tidal stress and jet observations. Current observational data may not be able to conclusively identify inactive source regions. For observation K at source region I, no activity is seen even though the viewing geometry should be favorable for its detection (Spitale and Porco, 2007). Based on Spitale and Porco (2007), this observation may be a positive detection of no or low activity. This region would be in compression, and therefore, not as likely to be highly active. Moreover, the minimum compressive stress is on the order

of the shear stress so shear failure would also be less likely. Thus, if this non-detection of activity is real, it is also consistent with the scenarios of tidal control of activity described here. This example also illustrates how non-detections are an important constraint when modeling the tidal control of jets.

A particularly energetic jet may modify its conduit, making it difficult for tidal stress to completely restrict eruption activity. Thus, a specific source region may always be active at some level throughout the orbit and the role of tidal stress will be to modulate eruption rates as specific conduits to the surface are dilated and constricted throughout Enceladus' orbit. Thus, future Cassini ISS analysis of jet observations should also try to quantify the amount of material being erupted by specific jets at the times of observations. The observations of activity combined with eruption rates can further solidify the links between tidal stress state and observed activity on Enceladus.

Looking at the south polar region as a whole, it might be possible that jet activity never ceases entirely at any point in Enceladus' orbit. Even though tidal stress might limit activity at any given source region; other source regions with different geometries might be active at that time. Therefore, we should not expect to find a time in which no jet is actively venting into space. However, again the total volume of the material being vented is likely to be variable. In fact, Cassini Ultraviolet Imaging Spectrograph (UVIS) observations seem to indicate that total venting rates can vary by at least about a factor of 2 (Hansen et al., 2008).

With information about when in Enceladus' orbit specific jets are active and inactive, along with eruptions rates during times of activity, we can start to determine whether and how tidal stress might affect the venting of volatile material. Once the geological mechanism that correlates best with eruption activity is identified, we can further refine our tidal stress model to provide the best fit to the observations. For example, it has been shown that obliquity can change the tidal stress on a satellite (Hurford et al., 2009b; Jara-Orué and Vermeersen, 2011) and a systematic survey of the effect of obliquity on stress in the source regions could also be conducted.

Moreover, the model of stress employed here is an elastic model. If any part of the ice shell responds in a viscoelastic way, which is possible even though the timescale for diurnal stress is below the Maxwell time for ice, then a lag in the tidal stress may be seen. Such a lag may affect when the transitions from compression to tension occur, a potentially important consideration in future work.

In conclusion, we find that a link between tidal stress and observations of eruption activity is plausible. Further, high-resolution, high-phase jet observations can be used to solidify this link. Tying the control of eruption activity to the tidal stress state has implications for the depth at which volatiles are building up before release, since overburden pressure limits the depths to which tidal stress is able to produce geological motions.

References

Greenberg, R., Geissler, P., Hoppa, G., Tufts, B.R., Durda, D.D., Pappalardo, R., Head, J.W., Greeley, R., Sullivan, R., Carr, M.H., 1998. Tectonic processes on Europa: Tidal stresses, mechanical response, and visible features. Icarus 135 (September), 64–78.
Hansen, C.J. et al., 2008. Water vapour jets inside the plume of gas leaving Enceladus. Nature 456 (November), 477–479.

Hoppa, G.V., Randall Tufts, B., Greenberg, R., Hurford, T.A., O'Brien, D.P., Geissler, P.E., 2001. Europa's rate of rotation derived from the tectonic sequence in the Astypalaea region. Icarus 153 (September), 208–213.

Howett, C.J.A., Spencer, J.R., Pearl, J., Segura, M., 2011. High heat flow from Enceladus' south polar region measured using 10–600 cm⁻1 Cassini/CIRS data. J. Geophys. Res. (Planets) 116 (March), 3003.

Hurford, T.A., Helfenstein, P., Hoppa, G.V., Greenberg, R., Bills, B.G., 2007a. Eruptions arising from tidally controlled periodic openings of rifts on Enceladus. Nature 447, 292–294.

Hurford, T.A., Sarid, A.R., Greenberg, R., 2007b. Cycloidal cracks on Europa: Improved modeling and non-synchronous rotation implications. Icarus 186 (January), 218–233.

Hurford, T.A., Bills, B.G., Helfenstein, P., Greenberg, R., Hoppa, G.V., Hamilton, D.P., 2009a. Geological implications of a physical libration on Enceladus. Icarus 203 (October), 541–552.

Hurford, T.A., Sarid, A.R., Greenberg, R., Bills, B.G., 2009b. The influence of obliquity on European cycloid formation. Icarus 202 (July), 197–215.

Jara-Orué, H.M., Vermeersen, B.L.A., 2011. Effects of low-viscous layers and a non-zero obliquity on surface stresses induced by diurnal tides and non-synchronous rotation: The case of Europa. Icarus 215 (September), 417–438.

Leith, A.C., McKinnon, W.B., 1996. Is there evidence for polar wander on Europa? Icarus 120 (April), 387–398.

Melosh, H.J., 1977. Global tectonics of a despun planet. Icarus 31 (June), 221–243.

Nimmo, F., Spencer, J.R., Pappalardo, R.T., Mullen, M.E., 2007. Shear heating as the origin of the plumes and heat flux on Enceladus. Nature 447, 289–291.

Patthoff, D.A., Kattenhorn, S.A., 2011. A fracture history on Enceladus provides evidence for a global ocean. Geophys. Res. Lett. 38 (September), 18201.

Porco, C.C. et al., 2006. Cassini observes the active south pole of Enceladus. Science 311 (March), 1393–1401.

Porco, C. et al., 2011. Jetting activity and thermal emission across the south polar terrain of Enceladus: Observations and comparisons with shear-heating models AGU Fall Meeting Abstracts, F2.

Smith-Konter, B., Pappalardo, R.T., 2008. Tidally driven stress accumulation and shear failure of Enceladus's Tiger Stripes. Icarus 198 (December), 435–451.

Sohl, F., Hussmann, H., Ziethe, R., 2006. Interior structures of Enceladus and Mimas: Implications from their densities and equilibrium shapes. In: Bulletin of the American Astronomical Society, vol. 38. p. 521.

Spencer, J.R. et al., 2006. Cassini encounters Enceladus: Background and the discovery of a south polar hot spot. Science 311, 1401–1405.

Spitale, J.N., Porco, C.C., 2007. Association of the jets of Enceladus with the warmest regions on its south-polar fractures. Nature 449, 695–697.

Zhang, K., Nimmo, F., 2009. Internal structure of Enceladus and dione from orbital constraints. Lunar Planet. Sci. 40, 2199.